A Polarization-Reconfigurable Glass Dielectric Resonator Antenna Using Liquid Metal

Zhe Chen, Hang Wong and James Kelly

***Abstract*—In this communication, we introduce a glass dielectric resonator antenna (DRA) incorporating a liquid-metal polarizer capable of polarization reconfiguration. The polarizer is formed by a type of liquid-metal alloy composed of gallium, indium, and tin. The antenna is capable of generating three different polarizations: a – 45° polarization (STATE 1), a + 45° polarization (STATE 2) and a *y*-axis polarization (STATE 3). The glass DRA is designed to operate at 2.4 GHz with a wide effective bandwidth (overlapped impedance bandwidths of the three states) of 18.0 % and a high radiation efficiency of more than 80 %. The experimental results agree well with the theoretical analyses.**

***Index Terms*—polarization reconfiguration, glass DRA, liquid metal, polarizer.**

I. Introduction

Polarization-reconfigurable antennas [1]-[8] have been introduced in recent decades. Polarization reconfiguration has been demonstrated within various different types of antennas such as: monopole [6], dipole [3], slot [7], and patch antennas [1]-[2]. Polarization-reconfigurable antennas have numerous applications within wireless communication systems, including: 1) modulation [4], 2) enhancing the quality and capacity of a channel in a multiple input multiple output (MIMO) system [5], 3) alleviating fading losses caused by multipath effects [6], and 4) helping to mitigate for signal depolarization within a wireless propagation channel [8]. This reduces the polarization mismatch and hence improves SINR (Signal to Interference plus Noise Ratio).

Dielectric resonator antennas (DRAs) have the unique feature that the radiation is emitted from dielectric radiators rather than metallic radiators. Several designs have been reported, in the literature, for DRAs realizing various forms of reconfiguration. In reference [9]-[11], liquid dielectrics were employed to reconfigure the: operating frequency [9], radiation pattern [10], and polarization [11] of DRAs. For the first time we present a glass DRA incorporating a liquid-metal polarizer. Glass DRAs were first proposed in [12] and offer various advantages in comparison with the use of other dielectric materials. The structure of a DRA lends itself well to polarization reconfiguration which can be achieved simply by disturbing the electromagnetic-field distribution associated with the DRA. Inspired by previous research on liquid-metal antennas [16]-[19], we chose to inject liquid-metal alloy into a glass DRA in order to redistribute the electromagnetic-field, thus resulting in polarization reconfiguration.

To the best of our knowledge, this design is the first to demonstrate liquid metal can be used to create a DRA capable of polarization reconfiguration. The proposed antenna affords a wide effective bandwidth (overlapped bandwidths of the three operating states) of 18.0 % along with a radiation efficiency in excess of 80 %.

This communication is organized as follows. Section II introduces underlying theory, design, and construction of the proposed antenna. Section III discusses the simulated and measured performance of the proposed antenna. Finally, a conclusion is drawn in Section IV.

Manuscript received 27 October 2018.
This project was supported in part by the Research Grant Council of the Hong Kong SAR, China under Project CityU11266416.

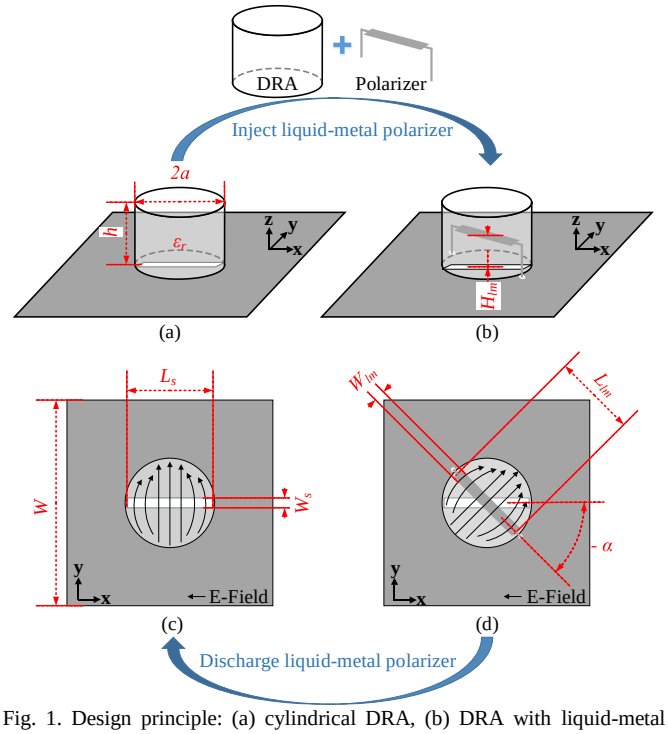

Fig. 1. Design principle: (a) cylindrical DRA, (b) DRA with liquid-metal polarizer, (c) electric-filed distribution of DRA, and (d) electric-filed distribution of DRA with liquid-metal polarizer.

II. Antenna Design and Fabrication

This section presents the underlying theory, design principles, geometry and construction of the proposed antenna. In addition, we also justify the choice of materials and the fabrication technique.

A. Antenna Design

Fig. 1 shows the construction of the proposed antenna. The antenna consists of a glass DRA mounted above a ground plane incorporating an aperture. Energy is coupled from a microstrip transmission line, printed on the underside of the ground plane, through the aperture, and into the DRA. The DRA is excited in the fundamental $HE_{11\delta}$ mode. When operated in this mode the DRA behaves as a short horizontal magnetic dipole [15]. The electric-field distribution associated with this mode is sketched in Fig. 1 (c). This distribution is identical to that of a regular cylindrical-DRA [15]. It provides broadside radiation and the electric field is polarized along the *y*-axis. Then a small quantity of liquid-metal is injected into the DRA, as shown in Fig. 1 (b). The liquid-metal structure consists of a horizontal part (in the *x*-*y* plane) and 2 vertical parts. The metalic polarizer, thus formed, is orientated at an angle of $-\alpha$ with respect to the aperture in the ground plane. The

Zhe Chen and Hang Wong are with the State Key Laboratory of Millimeter Waves, Department of Electronic Engineering, City University of Hong Kong, (email: hang.wong@cityu.edu.hk).
J. R. Kelly is with the School of Electronic Engineering and Computer Science, Queen Mary University of London, UK (email: j.kelly@qmul.ac.uk).

presence of the metallic polarizer rotates the electric-field distribution clockwise by an angle of α, as shown in Fig. 1 (d). The polarization of the DRA is thus transformed from 0° (before injection) to α (after injection).

A resonant frequency appears at 2.85 GHz when the liquid-metal polarizer is presented, as shown in Fig. 2 (a). Fig. 2 (b) shows the surface-current and electric-field distributions on the polarizer at 2.4 GHz and 2.85 GHz. First let us concentrate on the polarization change in the DRA. Field coupled through the aperture in the ground plane induces a surface current on the polarizer. This induced current has the effect of varying the electric-field distribution within the DRA. Since the polarization of the radiating wave is determined by the direction of the electric field generated within the DRA, we can use the orientation of the polarizer to control the electric-field distribution as well as the polarization of radiation wave. According to the electric field distribution on the polarizer, as shown in Fig 2 (b), the polarization of the electric-field is orthogonal to the horizontal arm of the polarizer. The physical electrical length of the polarizer is defined as l_{elc}. To reduce the radiation influence of the polarizer to the DRA, l_{elc} was chosen slightly longer than λ_g at 2.4 GHz. From the current distribution of the polarizer at 2.4 GHz as shown in Fig. 2 (b), the polarizer is not resonant at 2.4 GHz. Since l_{elc} is close to $1.5\cdot\lambda_g$ at 2.85 GHz which satisfy the resonant condition of the polarizer at 2.85 GHz. From the current distribution of the polarizer, strong currents condense along the edges and the pipes of the horizontal strip of the polarizer. We may conclude that the polarizer performs as a non-resonant polarizer at 2.4 GHz while a radiator at 2.85 GHz. We did not include this additional resonant mode from the polarizer at 2.85 GHz in the operating bandwidth of the proposed antenna. We can tune the resonant frequency of the polarizer at 2.85 GHz by adjusting l_{elc}. The only method to adjusting l_{elc} is to tune the polarizer height (H_{lm}). Increasing H_{lm} from 10 to 16 mm does not affect the resonant frequency of the DRA. However, the resonant frequency of the polarizer shifts to the lower frequency band, as shown in Fig. 2 (c). When the resonant frequency of polarizer coincides with the frequency of the DRA mode, the interference of the electric fields between the polarizer and DRA modes together with a proper phase-difference would lead to circular or elliptical polarization, thus resulting in a poor linear polarization purity. On the contrary, if we want to move the resonant frequency of polarizer away from the DRA mode, we need to lower the polarizer height, which means the polarizer must be bought closer to the aperture. Unfortunately, this has a detrimental effect on the impedance matching. H_{lm} = 10 mm was selected because this represents a good compromise between the two extreme conditions described above.

According to the above analysis, the electric-field associated with the $HE_{11\delta}$ mode is always orthogonal to the horizontal arm of the polarizer, as shown in Fig. 3. Altering the angles α, thus reconfigures the polarization of the DRA. In this communication we validate our approach, for varying the polarization of a DRA, by setting $\alpha = \pm 45°$ because many applications need the antenna having an ability of tuning the polarization between two orthogonal polarization states.

The dimensions of the cylindrical DRA were calculated using the following formulas [15]:

$$k_0 \cdot a = \frac{6.324}{\sqrt{\varepsilon_r + 2}} \cdot \left[0.27 + 0.36 \cdot \frac{a}{2h} + 0.02 \cdot \left(\frac{a}{2h} \right)^2 \right] \quad (1)$$

$$k_0 \cdot a = \frac{f_{GHz} \cdot h_{cm} \cdot \frac{a}{h}}{4.7713} \quad (2)$$

We designed the antenna to operate at a resonant frequency f_0 of 2.4 GHz. The permittivity (ε_r) of the glass dielectric was 7.1.

In formulas 1 and 2, a and h are the radius and height of the cylindrical DRA, respectively, as shown in Fig. 1 (a). The computer simulations reported in this communication, were performed using

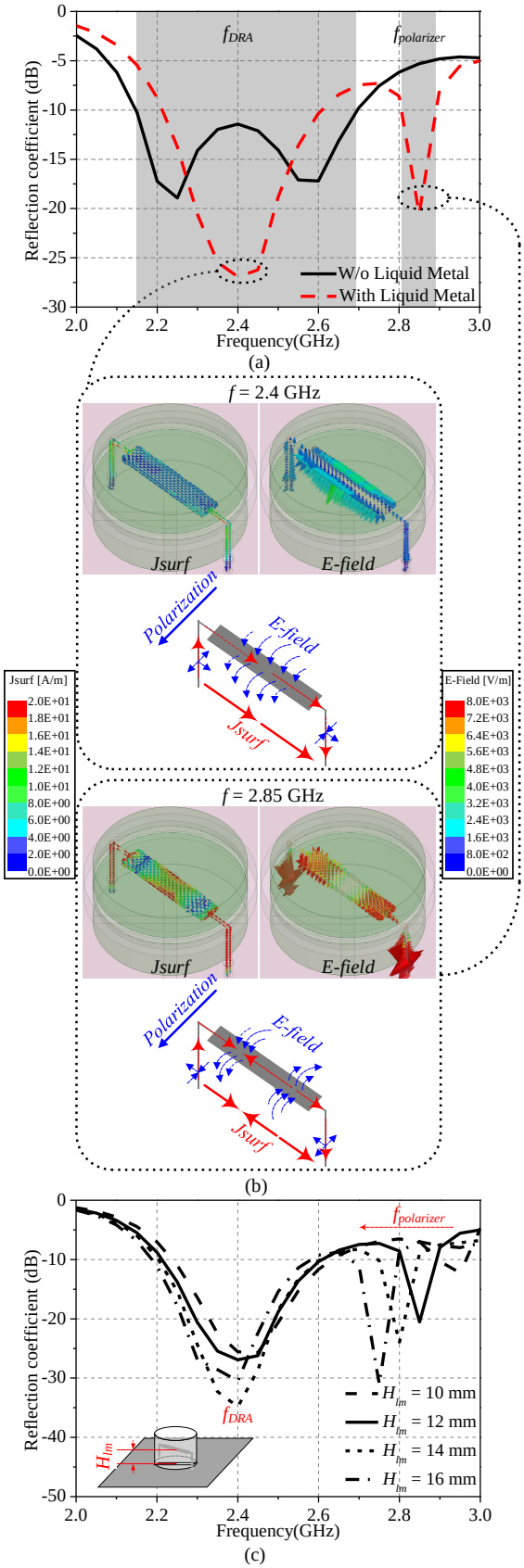

Fig. 2. The analysis of liquid-metal polarizer: (a) impedance matching, (b) surface-current and electric-field distributions and (c) height of polarizer.

Ansoft HFSS. The aperture is fed by a microstrip transmission line and the dimensions of the aperture and the microstrip line were determined

using guidance given in reference [15]. The final dimensions of the proposed antenna are shown in Table I.

B. Fabrication and Switch Control

Reference [12] describes the first use of a K9 glass dielectric material to create a transparent DRA. Using transparent materials to demonstrate our reconfigurable approach has the following advantages: 1) we can clearly observe the reconfigurable process to control the injecting switch; 2) the transparent DRA also can act as a decoration artwork. For the persons who worried about the radiation, this kind of design can avoid their psychological problems [13]-[14]. The dielectric constant and loss tangent of the K9 glass was measured in our lab (ε_r = 7.1 and loss tangent = 0.02 from 2 to 3 GHz), thus enabling it to be used within RF applications. In [16]-[19], various types of liquid metals have been employed to construct reconfigurable antennas. In this design, Galinstan was used.

In the interests of cost-effectiveness, the feed aperture was fabricated using traditional PCB technology. The microfluidic cavity was fabricated using a 3-D printer *Formlab 2*. The source material for the printer was *High Temp Resin* [20]. The dielectric constant and loss tangent of this material were measured in our lab. (ε_r = 2.6 and loss tangent = 0.01 from 2 to 3 GHz). The exploded view in Fig. 4 outlines the fabrication process in detail.

Pumps were integrated with the proposed antenna in order to actuate liquid metal and enable reconfiguration. Fig. 5 (a), illustrates the set-up. First let us consider operating STATE 1. Operating STATE 1 is obtained when liquid metal is injected into the microfluidic channel 1. STATE 1 yields + 45° polarization. Now let us consider operating STATE 2. Operating STATE 2 is obtained when the liquid metal is injected into the microfluidic channel 2. The antenna generates − 45° polarization. Finally, if both the of the microfluidic channels are empty the antenna yields linear polarization aligned with the *y*-axis.

C. Repeatability

Considering the drawbacks of Galinstan such as: oxidization and stiction, it is important to examine the longevity and repeatability of this design. However, one can still observe some stiction of Galinstan to the inner surface of the container as seen in Fig. 5 (b). The weak surface tension of Galinstan together with the rough surface of the 3-D-printed container contribute to the stiction problem.

To address the stiction problem, the residual Galinstan was evacuated using a dilute HCl solution [16] or by rinsing with a Teflon solution [17]. During the experiment, we also repeated the measurement several times. On each occasion we emptied and cleaned the container using a dilute HCl solution. This did not lead to any observable differences in the measurement results. However, the necessity for cleaning currently limits the applications of the technology. Reference [18] demonstrated reconfiguration inside an Inert Lab. Glove Box to avoid the stiction. However, a need for a special working environment would limit the practical applications of the technology. In [19] the liquid metal was surrounded by NaOH in order to avoid stiction. However, a potential leakage of NaOH liquid is a potential cause for concern with that approach. Further work is required to perfect techniques for alleviating the stiction problem. This is inherently interdisciplinary work requiring significant input from chemistry specialists.

III. Antenna Performance

In the experiment, reflection coefficients in three states were measured using an *Agilent* 8753 vector network analyzer. In addition, a *Satimo StarLab* system was employed in order to measure the radiation performance of the antenna (namely: the radiation patterns, realized gain, and radiation efficiency) in each of the three operating states.

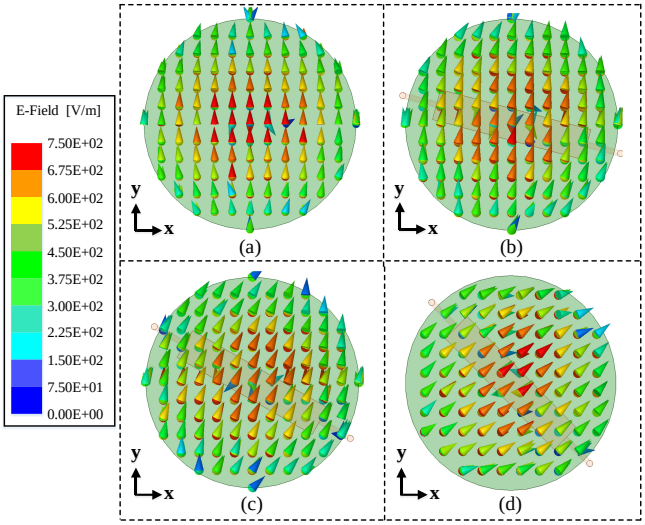

Fig. 3. Simulated electric-field distributions in the DRA: (a) no liquid metal, (b) α = 15°, (c) α = 30°, and (d) α = 45°.

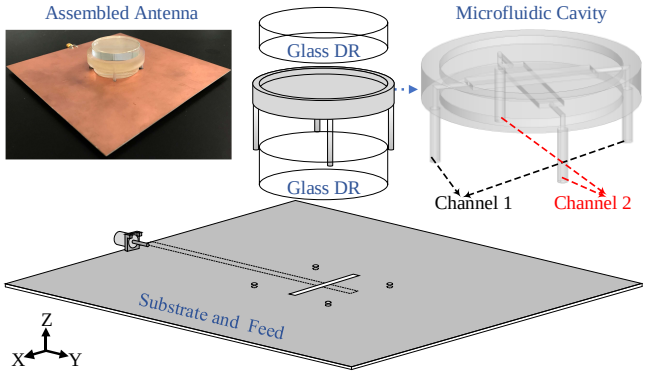

Fig. 4. Exploded view of the proposed polarization-reconfigurable glass DRA.

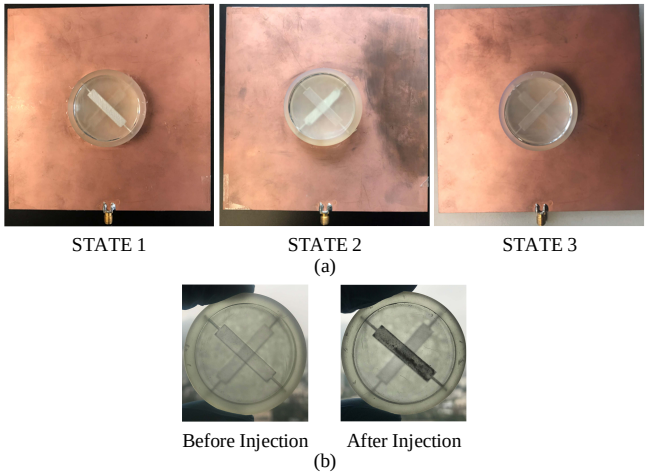

Fig. 5. Reconfiguration process: (a) working states and (b) stiction problem.

TABLE I
DESIGN PARAMETERS OF THE PROPOSED ANTENNA

a	h	W	L_s	W_s	H_{lm}	W_{lm}	L_{lm}
20.5 mm	23.4 mm	140 mm	40 mm	3 mm	10 mm	6 mm	30 mm

A. *Reflection Coefficient*

Fig. 6 shows the simulated and measured reflection coefficients for the three operating states.

In STATE 1 (+ 45° polarization), black solid and dashed lines with square symbols represent the simulated and measured reflection coefficients, respectively. Based on the measured results, the impedance bandwidth (reflection coefficient < -10 dB) for STATE 1 is 18.0 % from 2.22 GHz to 2.66 GHz.

In STATE 2 (− 45° polarization), red solid and dashed lines with circular symbols represent the simulated and measured reflection coefficients, respectively. According to the measured results, the impedance bandwidth for STATE 2 is 20.0 % from 2.21 GHz to 2.70 GHz.

In STATE 3 (*y*-axis polarization), blue solid and dashed lines with triangular symbols represent the simulated and measured reflection coefficients, respectively. The measured impedance bandwidth for STATE 3 is 23.2 % from 2.13 GHz to 2.69 GHz.

For both operating states, simulation and measurement are in good agreement. Finally, the effective bandwidth (overlapped grey area) for the proposed antenna is 18.0 % from 2.22 GHz to 2.66 GHz.

B. *Radiation Pattern*

Fig. 7 compares the simulated and measured radiation patterns for the three operating states, at the 2.4 GHz. There is a good agreement between simulation and measurement.

In Fig. 7, the black solid and dashed lines are used to represent the simulated co-polar and cross-polar radiation patterns, respectively. Additionally, red dash-dotted and short-dashed lines are used to display measured co-polar and cross-polar radiation patterns, respectively. However, the simulated cross-polar radiation patterns could not be plotted for STATE 3 because the magnitude is less than -30 dB. The magnitude of cross-polar radiation associated with STATEs 1 and 2 is larger than that associated with STATE 3, due to radiating-contributions from the vertical part of the liquid-metal polarizer, as shown in Fig. 2 (b). The antenna yields broadside radiation patterns in both states, as expected.

C. *Gain and Efficiency*

Fig. 8 presents the simulated and measured realized-peak gains along with the radiation efficiencies, associated with the three operating states. Black solid and dashed lines with square symbols are used to represent STATE 1. Red solid and dashed lines with circular symbols show STATE 2. Blue solid and dashed lines with triangular symbols display STATE 3. There are good agreements between simulations and measurements for all of the states. It can be observed that the measured curves, shown in Fig. 8, lie slightly below the simulated curves. This can be attributed to an error in the measured value of the material losses. In the simulation, the loss tangent of the glass material was set to 0.02. This value was obtained through measurement using an *Agilent* 85070D Dielectric Probe Kit [21]. A measurement error of ± 0.05 is expected in the value of the loss tangent. As a result, the drops of gains and radiation efficiencies in the measurement are reasonable.

Fig. 8 shows that the measured gains of the antenna are greater than 6 dBi for the three operating states. Additionally, the measured radiation efficiencies are over 80 % for the three operating states. Although the conductivity of Galinstan is one order lower than that of copper, the antenna gains and radiation efficiencies do not decrease excessively. This result indicates that the radiating power mostly comes from the $HE_{11\delta}$ mode of the DRA rather than the polarizer mode. We may conclude, therefore that the resistive loss of the polarizer does not adversely affect the radiation efficiencies and gains of the antenna.

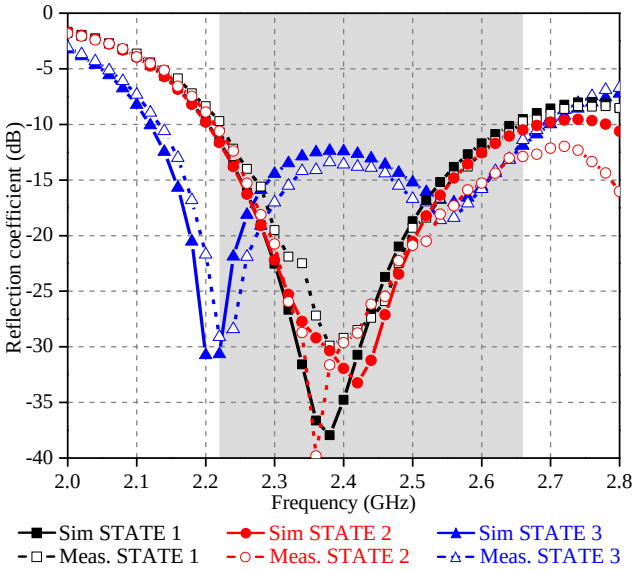

Fig. 6. Measured and simulated reflection coefficients in three states.

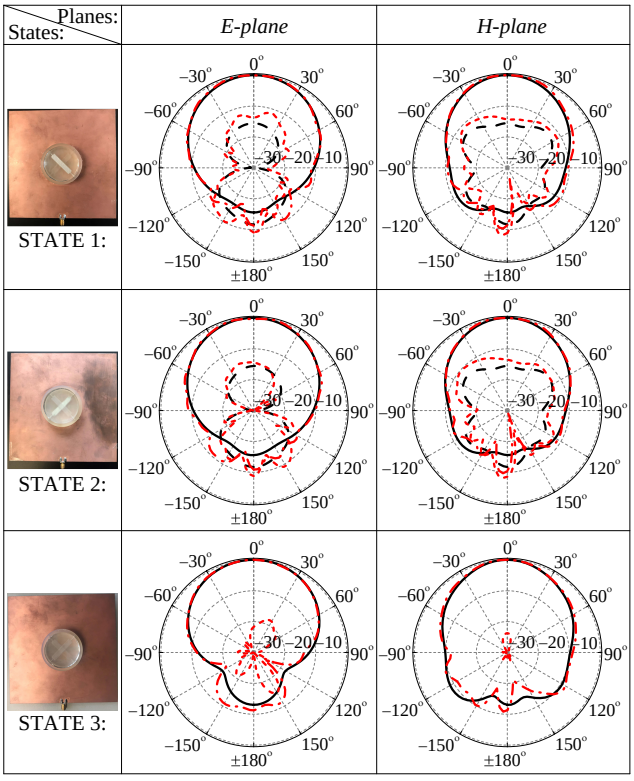

Fig. 7. Measured and simulated radiation patterns in three states.

Traditional approaches for reconfiguring antennas are not applicable to DRAs. For example, the integration of p-i-n diodes leads to a gain drop together with lower radiation efficiency. Table II lists measured peak gains and efficiencies of state-of-the-art reconfigurable DRA designs in comparison with the proposed antenna. By contrast, a liquid-metal reconfigurable DRA has better gain and radiation efficiency than one incorporating p-i-n-diodes. However, the performance of these two types of reconfigurable antenna should be evaluated according to the demands of a particular application that the engineer has in mind. The reconfigurable DRAs incorporating p-i-n-

TABLE II
COMPARISON FOR ANTENNA PERFORMANCE

Ref.	Reconfigurable Categories	Peak Gain (measurement)	Radiation Eff. (measurement)
[22]	Polarization	7.35 - 7.5 dBi	66 - 73 %
[23]	Frequency	1.04 – 1.69 dBi	NULL
[24]	Frequency	3.52 -4.86 dBi	60 -70 %
[25]	Frequency	NULL	47 - 58 %
[26]	Frequency	2.6 - 4.6 dBi	54 %
Our work	**Polarization**	**> 6 dBi**	**> 80 %**

diodes have faster switching speed but lower gains and radiation efficiencies. However reconfigurable DRAs incorporating liquid-metal offer better radiating efficiencies and gains at the expense of slower reconfiguration speed.

D. Thermal Effect

Liquid metals exhibit a relatively high thermal coefficient of expansion. For this reason, thermal effects might impose limitations on the practical applications of liquid-metal antennas. The last phase of the experiment therefore involves measuring the proposed antenna in a thermal test chamber (MC-810, *MINI-SUBZERO*). The set-up of the experiment is shown in Fig. 9 (a), the proposed antenna is placed in the thermal chamber. The internal temperature of the chamber is varied, meanwhile, a portable VNA (MS2038C, *ANRITSU*) is employed to monitor the reflection coefficients of the antenna.

In Fig. 9 (b), black lines show the measured results obtained in the air while the colored lines represent measured results obtained in the thermal chamber, at different temperatures, ranging from 10 ℃ to 50 ℃. Compared with smooth curves obtained in the air, one can observe additional ripples on measured the reflection coefficients obtained within the thermal chamber. This is not a temperature induced effect but is caused by the presence of multiple reflection from the metallic walls of the chamber. It can therefore be concluded that the reflection coefficient of the proposed antenna is relatively insensitive to a temperature-variations.

IV. CONCLUSION

This communication presents a novel polarization-reconfigurable glass DRA. The antenna is able to switch its polarization between + 45°, − 45° and the *y*-axis direction by altering the flow of liquid metal within a polarizer embedded inside the DRA. The measurements and simulations were in good agreement. The proposed antenna has a wide effective bandwidth of 18.0 %. In addition, it has a higher gain and radiation efficiency than most reported reconfigurable DRAs incorporating p-i-n-diodes. Furthermore, to the best of our knowledge, the communication presents the first analysis of the effects of temperature on the reflection coefficient performance of a liquid metal antenna. For a potential application, the liquid-metal-type reconfigurable DRA could be used within a wireless detection system where different information is transmitted on different channels differing in their polarizations.

ACKNOWLEDGMENT

This project was supported in part by the Research Grants Council of the Hong Kong SAR, China (Project No. CityU 11266416). We would also like to acknowledge the support of the UK EPSRC (EP/P008402/1). The authors would like to thank the editors and reviewers for their review work and helpful comments.

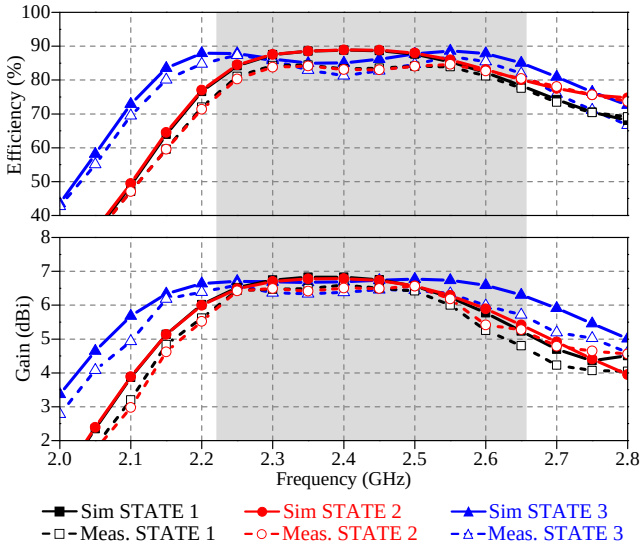

Fig. 8. Measured and simulated gains and efficiencies in three states.

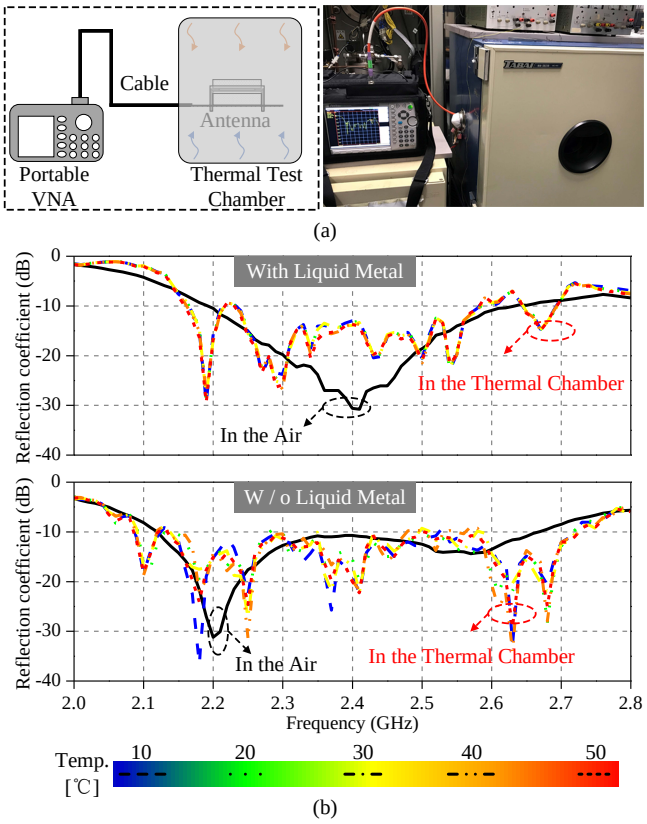

Fig. 9. Thermal-effect: (a) experimental set-up and (b) comparison of experimental results.

REFERENCES

[1] P. Y. Qin, A. R. Weily, Y. J. Guo and C. H. Liang, "Polarization reconfigurable U-slot patch antenna," *IEEE Trans. Antennas Propag.*, vol. 58, no. 10, pp. 3383-3388, Oct. 2010.

[2] S. L. Chen, F. Wei, P. Y. Qin, Y. J. Guo and X. Chen, "A multi-linear polarization reconfigurable unidirectional patch antenna," *IEEE Trans. Antennas Propag.*, vol. 65, no. 8, pp. 4299-4304, Aug. 2017.

[3] W. Yang, W. Che, H. Jin, W. Feng and Q. Xue, "A polarization-reconfigurable dipole antenna using polarization rotation AMC structure," *IEEE Trans. Antennas Propag.*, vol. 63, no. 12, pp. 5305-5315, Dec. 2015.

[4] M. A. Kossel, R. Kung, H. Benedickter and W. Biichtokd, "An active tagging system using circular-polarization modulation," *IEEE Trans. Microw. Theory Tech.*, vol. 47, no. 12, pp. 2242-2248, Dec. 1999.

[5] J. F. Valenzuela-valdes, M. A. Garcia-fernandez, A. M. Martinez-gonzalez and D. Sanchez-Hernandez, "The role of polarization diversity for MIMO systems under rayleigh-fading environments," *IEEE Antennas Wireless Propag. Lett*., vol. 5, no. 1, pp. 534-536, Dec. 2006.

[6] B. Liang, B. Sanz-Izquierdo, E. A. Parker and J. C. Batchelor, "A frequency and polarization reconfigurable circularly polarized antenna using active EBG structure for satellite navigation," *IEEE Trans. Antennas Propag.*, vol. 63, no. 1, pp. 33-40, Jan. 2015.

[7] Y. Li, Z. Zhang, W. Chen and Z. Feng, "Polarization reconfigurable slot antenna with a novel compact CPW-to-slotline transition for WLAN application," *IEEE Antennas Wireless Propag. Lett*., vol. 9, pp. 252-255, 2010.

[8] H. Wong, W. Lin, L. Huitema and E. Arnaud, "Multi-polarization reconfigurable antenna for wireless biomedical system," *IEEE Trans. Biomed. Circuit Syst*., vol. 11, no. 3, pp. 652-660, June 2017.

[9] G. H. Huff, D. L. Rolando, P. Walters and J. McDonald, "A frequency reconfigurable dielectric resonator antenna using colloidal dispersions," *IEEE Antennas Wireless Propag. Lett*., vol. 9, no., pp. 288-290, 2010.

[10] Z. Chen and H. Wong, "Wideband glass and liquid cylindrical dielectric resonator antenna for pattern reconfigurable design," *IEEE Trans. Antennas Propag.*, vol. 65, no. 5, pp. 2157-2164, May 2017.

[11] Z. Chen and H. Wong, "Liquid dielectric resonator antenna with circular polarization reconfigurability," *IEEE Trans. Antennas Propag*., vol. 66, no. 1, pp. 444-449, Jan. 2018.

[12] E. H. Lim and K. W. Leung, "Transparent dielectric resonator antennas for optical applications," *IEEE Trans. Antennas Propag*., vol. 58, no. 4, pp. 1054-1059, April 2010.

[13] K. W. Leung, Y. M. Pan, X. S. Fang, E. H. Lim, K. M. Luk and H. P. Chan, "Dual-function radiating glass for antennas and light covers—part I: omnidirectional glass dielectric resonator antennas," *IEEE Trans. Antennas Propagat.*, vol. 61, no. 2, pp. 578-586, Feb. 2013.

[14] K. W. Leung, X. S. Fang, Y. M. Pan, E. H. Lim, K. M. Luk and H. P. Chan, "Dual-function radiating glass for antennas and light covers—part II: dual-band glass dielectric resonator antennas," *IEEE Trans. Antennas Propagat*., vol. 61, no. 2, pp. 587-597, Feb. 2013.

[15] A. Petosa, *Dielectric Resonator Antenna Handbook*. Norwood, MA, USA: Artech House, 2007.

[16] G. H. Huff, H. Pan, D. J. Hartl, G. J. Frank, R. L. Bradford and J. W. Baur, "A physically reconfigurable structurally embedded vascular antenna," *IEEE Trans. Antennas Propag*., vol. 65, no. 5, pp. 2282-2288, May 2017.

[17] A. Pourghorban Saghati, J. Singh Batra, J. Kameoka and K. Entesari, "Miniature and reconfigurable CPW folded slot antennas employing liquid-metal capacitive loading," *IEEE Trans. Antennas Propag*., vol. 63, no. 9, pp. 3798-3807, Sept. 2015.

[18] A. Dey, R. Guldiken and G. Mumcu, "Microfluidically reconfigured wideband frequency-tunable liquid-metal monopole antenna," *IEEE Trans. Antennas Propag*., vol. 64, no. 6, pp. 2572-2576, June 2016.

[19] G. B. Zhang, R. C. Gough, M. R. Moorefield, K. J. Cho, A. T. Ohta and W. A. Shiroma, "A liquid-metal polarization-pattern-reconfigurable dipole antenna," *IEEE Antennas Wireless Propag. Lett*., vol. 17, no. 1, pp. 50-53, Jan. 2018.

[20] 3-D printing material. Available: https://support.formlabs.com/hc/en-us/articles/115000015650-Using-High-Temp-Resin

[21] 85070D Dielectric Probe Kit Product. *Agilent Corp.* [Online]. Available: http://www.mit.pref.miyagi.jp/emc/Network-analyzer/5968-5330E.pdf

[22] W. W. Yang, X. Y. Dong, W. J. Sun and J. X. Chen, "Polarization reconfigurable broadband dielectric resonator antenna with a lattice structure," *IEEE Access*, vol. 6, pp. 21212-21219, 2018.

[23] S. Danesh, S. K. A. Rahim, M. Abedian and M. R. Hamid, "A compact frequency-reconfigurable dielectric resonator antenna for LTE/WWAN and WLAN applications," *IEEE Antennas Wireless Propag. Lett*., vol. 14, pp. 486-489, 2015.

[24] S. Danesh, S. K. A. Rahim, M. Abedian, M. Khalily and M. R. Hamid, "Frequency-reconfigurable rectangular dielectric resonator antenna," *IEEE Antennas Wireless Propag. Lett.*, vol. 12, pp. 1331-1334, 2013.

[25] J. B. Yan and J. T. Bernhard, "Implementation of a frequency-agile MIMO dielectric resonator antenna," *IEEE Trans. Antennas Propag*., vol. 61, no. 7, pp. 3434-3441, July 2013.

[26] J. Desjardins, D. A. McNamara, S. Thirakoune and A. Petosa, "Electronically frequency-reconfigurable rectangular dielectric resonator antennas," *IEEE Trans. Antennas Propag*., vol. 60, no. 6, pp. 2997-3002, June 2012.